Available online at www.sciencedirect.com
ScienceDirect
ISPRS Journal of Photogrammetry & Remote Sensing 62 (2007) 415–433
PHOTOGRAMMETRY & REMOTE SENSING
www.elsevier.com/locate/isprsjprs

Correction of laser scanning intensity data: Data and model-driven approaches

Bernhard Höfle [a,b,*], Norbert Pfeifer [a,c]

[a] alpS-Centre for Natural Hazard Management, Grabenweg 3, 6020 Innsbruck, Austria
[b] Institute of Geography, University of Innsbruck, Innrain 52, 6020 Innsbruck, Austria
[c] Institute of Photogrammetry and Remote Sensing, Vienna University of Technology, Gusshausstrasse 27-29, 1040 Vienna, Austria

Received 23 November 2006; received in revised form 7 May 2007; accepted 23 May 2007
Available online 16 July 2007

Abstract

Most airborne and terrestrial laser scanning systems additionally record the received signal intensity for each measurement. Multiple studies show the potential of this intensity value for a great variety of applications (e.g. strip adjustment, forestry, glaciology), but also state problems if using the original recorded values. Three main factors, a) spherical loss, b) topographic and c) atmospheric effects, influence the backscatter of the emitted laser power, which leads to a noticeably heterogeneous representation of the received power. This paper describes two different methods for correcting the laser scanning intensity data for these known influences resulting in a value proportional to the reflectance of the scanned surface. The first approach – data-driven correction – uses predefined homogeneous areas to empirically estimate the best parameters (least-squares adjustment) for a given global correction function accounting for all range-dependent influences. The second approach – model-driven correction – corrects each intensity independently based on the physical principle of radar systems. The evaluation of both methods, based on homogeneous reflecting areas acquired at different heights in different missions, indicates a clear reduction of intensity variation, to 1/3.5 of the original variation, and offsets between flight strips to 1/10. The presented correction methods establish a great potential for laser scanning intensity to be used for surface classification and multi-temporal analyses.

Keywords: Laser scanning; Signal intensity; Reflectance; Correction

1. Introduction

Airborne Laser Scanning (ALS) provides a well accepted operational method for the acquisition of topographic data. Fundamental knowledge about the accuracy of this method (Baltsavias, 1999b) and the quality of produced digital elevation data sets (Kraus et al., 2004) has evolved in recent years and thus has opened the use of ALS to a wide range of applications. A lot of research effort has been put into the development of new algorithms for processing the primary result of ALS — the 3D point cloud (x,y,z). A great variety of filter algorithms has been published for the derivation of digital terrain models (DTMs) and for the segmentation and classification of laser points based on the spatial relationship, i.e. purely the geometrical

* Corresponding author. alpS-Centre for Natural Hazard Management, Grabenweg 3, 6020 Innsbruck, Austria. Tel.: +43 512 507 5428; fax: +43 512 507 2895.
E-mail addresses: bernhard.hoefle@uibk.ac.at (B. Höfle), np@ipf.tuwien.ac.at (N. Pfeifer).

0924-2716/$ - see front matter © 2007 International Society for Photogrammetry and Remote Sensing, Inc. (ISPRS). Published by Elsevier B.V. All rights reserved.
doi:10.1016/j.isprsjprs.2007.05.008

component, in the 3D point cloud (Filin and Pfeifer, 2006; Sithole and Vosselman, 2004). Algorithms and methods, also including optical information, for building extraction resulting in 3D city models as well as forest measurements, were developed (Hyyppä et al., 2004; Kaartinen et al., 2005).

This active remote sensing technique delivers not only detailed information about the geometry, but also about the reflectance characteristics of the Earth's surface in the laser wavelength, which is typically in the near infrared (NIR) spectra between wavelengths 800 nm and 1550 nm. Most ALS systems currently record the return amplitude of each received echo and a growing number of systems already provide full-waveform digitization (Persson et al., 2005). The emitted laser shot interacts with the surface, generating the backscatter, and the received signal is recorded as function of time. This signal can contain one or more peaks, which correspond to distinct reflections of the laser beam. In the field of ALS the terms signal intensity, reflectance intensity and pulse reflectance are often used as synonym for the return amplitude or energy of one echo. Our aim is to correct the value referred to as 'intensity', typically not well specified by the laser scanner manufacturers, in order to obtain a value proportional or equal to surface reflectance.

The benefit of ALS intensity has been studied in several different fields of applications, for example in forestry and glaciology, where the signal intensity is already used as additional data source for surface classification and object detection. As well as the fact that the intensity is already delivered to most end-users, the advantages of the active sensor system and its specific wavelength in the NIR also generates potential for using ALS intensity. The intensity values are available as attributes for the geometry (x,y,z,I) and in comparison to raw digital images typically already georeferenced (Filin, 2003; Kager, 2004). Ortho-rectified intensity images can be easily produced; they are insensitive to light conditions to a great extent, e.g. solar irradiation, clouds, illumination shadows, and support surface classification where a good spectral separability is given in the NIR (Wolfe and Zissis, 1993).

Most ALS systems recording the intensity are small-footprint scanners, which operate with a beam divergence in the range of 0.3 to 0.8 mrad and a flying altitude above ground up to 3500 m. With a beam divergence[1] of 0.8 mrad and a flying height of 1000 m, the laser footprint diameter would be 0.8 m (and 2.8 m for 3500 m flying height). The illuminated area covered by the footprint can be seen as the maximum achievable spatial resolution in terms of reflectance information. As for cameras, the spatial resolution, i.e. the footprint area, may vary strongly with different ranges and scan angles of the laser beam caused by changes in the flying altitude and the topography of the scanned surface, as the beam divergence is constant within one flight mission. The variations in scan geometry lead to a scanning pattern, i.e. the point spacing along and across track, which does not allow for a homogeneous sampling of the whole area and results in a concurrent under-sampling (gaps) and over-sampling (overlapping footprints) (Baltsavias, 1999a). For further processing of the intensity in both the point cloud and in rasterized image formats, the intensity has to be corrected for the influences of topography and flying altitude.

The intensity data provided by current commercial systems offer a resolution of 8-bit, 12-bit or 16-bit. There is no detailed insight given into the proprietary pulse detection algorithms. The intensity may correspond to a specific amplitude of the detected echo, e.g. its maximum, but also to the integral of the returned signal over the pulse width. In full-waveform system echo detection however, the backscattered signal is digitized, with e.g. 1 ns sampling. Such full-waveform data sets allow for applying individual detection algorithms and waveform modeling (Jutzi and Stilla, 2006). Additionally to the determined amplitude, pulse width and returned energy are also provided for each echo. Therefore, full-waveform ALS data is also suitable for calibration, i.e. the observed laser intensities can be converted to values proportional to surface reflectance (Kaasalainen et al., 2005; Wagner et al., 2006). However, with fullwaveform laser scanning the target cross-section, i.e. the quantity σ in Eq. (3), can be determined free of assumptions, such as the assumption of Lambertian reflectors.

The need for normalized intensity values and images, respectively, is most obviously given for large ALS data sets containing strong elevation differences, as for example in high mountainous areas where uncorrected intensity images can hardly be used. Furthermore, multi-temporal analysis based on intensity requires a strategy to convert intensity to a relative but comparable measurement for different epochs with different conditions (e.g. ALS system, scan geometry, atmospheric conditions, etc.). A correction technique on point basis takes the advantage of the higher degree of information in the original data, such as the timestamps saved for every shot and relationships between laser points and plane positions. Time tagging does not only allow to link a

[1] Assuming a Gaussian profile the beam divergence is defined via those points where the energy drops to a factor of $1/e^2$ of the maximum energy in the beam middle.

ground reflection to the corresponding emitter position along the flight path, but also offers – in principle – the potential of considering time dependent changes of surface properties, e.g. due to water content. The original intensity value is not lost in the correction process but the corrected value is saved as additional attribute for every echo. Once the intensity attribute of the laser points is normalized, the interpolation of undistorted images is straightforward. The objectives and contributions of this paper are:

- to give a short but broad review of recent works and applications considering ALS intensity (Section 2.1),
- to summarize the basics of the physical principles of ALS systems for understanding intensity values and reflectance, respectively (Section 2.2),
- to introduce an empirical correction technique with data-driven parameter estimation, as well as a model-based correction technique exploiting the physical principles (Section 4),
- to identify and quantify the factors for intensity variations over areas with the same surface cover/material, to determine, for example, how the signal intensity of ALS systems is affected by scan geometry (Section 5),
- to assess the potential of corrected laser return intensity as independent and additional variable for surface classification and multi-temporal analyses (Section 6).

Contrary to other papers treating the intensity and range measurement in detail (e.g., Jutzi and Stilla, 2006), this paper starts from a practical point of view. Given unknown environmental conditions during the acquisition of data as well as undisclosed details of the commercial airborne laser scanning systems, this paper details which procedures are to be applied in order to correct intensity measurements for subsequent utilization. In Section 3 the data used is presented and Section 7 concludes the findings.

2. Background

2.1. Recent work considering ALS intensity

Ever since the works of Hug and Wehr (1997); Thiel and Wehr (1999), based on a continuous-wave ranging system, in which 'the reflectance criterion proved to be the most reliable of the discriminators' for the automatic detection and identification of topographic surface objects (Hug and Wehr, 1997), a number of authors concentrated on evaluating the use of pulsed ALS system intensities. Progress can be found in many different fields, which can be divided into two major scopes a) sensor related procedures (particularly estimation of planimetric offsets) and b) surface segmentation and classification methods (e.g. land-cover classification, forestry, glaciology and urban applications). The studies presented below cover both 1) algorithms that process the original point cloud directly and 2) image processing techniques based on interpolated intensity raster data.

Several authors propose methods for the estimation of planimetric offsets between ALS strips with the help of reflectance data. For these approaches no calibration is required because only relative values from the first to the second strip or between neighboring pixels are of interest. Additionally, an offset and a scale factor between the intensities can, e.g., be estimated during matching procedures. Matching of local intensity texture assists the determination of planimetric strip discrepancies in flat areas with non-existent height contrast. Burman (2000) uses height and reflectance images simultaneously to match strips and determine the offsets. Maas (2001, 2002) introduces a least-squares matching strip adjustment method that allows searching for tie points in ALS reflectance data. The intensity value simply replaces the height value in the least-squares matching for the determination of horizontal shift parameters. Vosselman (2002) suggests using the reflectance for the estimation of edge locations. Initial edges are detected by a straight line growing algorithm on a median filtered reflectance image. These initial values (edge location and reflectance values on either side of the edge) are used as input for reducing edge location errors by analytical modeling of the response of a laser beam to a gray value edge in the original laser point cloud.

Oude Elberink and Maas (2000) show the use of reflectance data in segmentation tasks with image processing techniques. As for strip adjustment, the reflectance complements the procedure for classifying ground level objects with low contrast texture and no extension into z-direction. Up to 70% detection accuracy could be reached for the classification of road, grassland and agricultural land. In the study of Song et al. (2002) the usability of ALS intensity data for land-cover classification is tested. The separability of the classes asphalt, grass, roofs and trees is shown for three different intensity images calculated from the point cloud through a) Inverse Distance Weight (IDW) interpolation, b) IDW with following median filtering and c) Kriging. The interpolation and filtering helps to overcome noise and enhances the spectral separability

of the chosen classes. Song et al. (2002) state the potential of intensity for land-cover classification, but better results could be reached if disturbing effects of scan geometry on the intensity are removed through normalization by the angle of incidence. In Matikainen et al. (2003) the classification of homogeneous areas segmented in the height image is assisted by the Gray Level Co-occurrence Matrix (GLCM) homogeneity of intensity. Building segments are separated from tree segments by assuming a higher homogeneity in the GLCM of height, GLCM of intensity and a longer average length of segment edges for buildings.

In the supervised parametric classification algorithm of Charaniya et al. (2004) the intensity is used as a feature describing the four surface categories; roads, grass, buildings and trees. Using the intensity feature along with height and height variation, i.e. geometric features, caused an improvement in the classification results. Using the luminance of a gray-scale aerial image as a forth feature slightly improves the results. One step in the method of Clode et al. (2004) for automatic road extraction makes use of the intensity to limit the candidate last pulse laser points to a subset, which fulfills the defined threshold for minimum and maximum intensity depending on the road material characteristics. Clode et al. (2005) additionally introduce an *intensity density* function that describes the ratio of number of points fulfilling the threshold to all points in the local neighborhood. Thus, the intensity density value reduces problems caused by noise in the intensity. The characteristics of power lines, i.e. low return intensities due to their small effective reflecting area, have been used by Clode and Rottensteiner (2005) as criteria to differentiate between first pulses on power lines and vegetation. Rottensteiner et al. (2005) fused laser intensity data with multi spectral images to create a pseudo-NDVI image from the intensity and the red band of the digital orthophoto. The calculated NDVI is used as indicator for vegetation. Also man-made objects, such as roofs, have high reflectance characteristics in the laser wavelength and therefore cause errors in the NDVI. Luzum et al. (2005) use elevation and intensity measurements of first and last returns to discriminate between two object classes, buildings and trees. Mean intensities and standard deviations of intensities are found to provide the largest distances in feature space, the best separability respectively for the two classes. A correlation between geometrically related parameters, particularly the scan angle, and other features (e.g. mean intensity of first pulse) is stated by the authors but nevertheless the overall separation and therefore the classification accuracy remain high.

In Lutz et al. (2003) the potential of intensity imaging to classify glacial surface types is explained and the influence of scanning geometry (range, angle of incidence, footprint size) on the intensity is evaluated. The use of maximum intensity values in strip overlapping areas eliminates the cross-path fading effects in laser infrared images, as stated by the authors. The chosen surface classes (snow, ice, rock, water) can be distinctly identified in the intensity images and surpass the orthophotos in distinguishing surface features.

Moffiet et al. (2005) give an overview of literature dealing with ALS intensity in the field of vegetation/forest analysis. The main objective is to find reliable correlations between tree species and forest biophysical properties on the one hand and return amplitudes on the other (Lim et al., 2003; Persson et al., 2006). Due to the characteristic of laser shots to be partly reflected in different parts of the vegetation, the emitted energy is distributed to multiple reflections. As they point out, the derivation of reflectance from the return amplitude is wrong if the effective target area (backscattering cross-section) of each echo is not considered. Moffiet et al. (2005) also show how the return intensity statistics, for example average and standard deviation, are affected by forest structure and how variables based on intensity statistics could be used for characterizing closure, spacing and type of foliage components within tree crowns. Despite the fact that the intensity is not radiometrically calibrated Watt and Wilson (2005) find 'LiDAR intensity is the best single measure for identifying different species and species mixtures'.

The DTM filter comparison of Sithole and Vosselman (2004) does not mention any method which makes use of reflectance data. Nevertheless, the intensity assists surface classification and therefore is of interest to the generation of DTMs.

Most studies listed above do not use the intensity data of laser points directly but derive variables from it (e.g. mean, standard deviation, 'intensity density' in a local neighborhood (as defined by Clode et al., 2005)) describing the target object features. Basically, the accuracy and quality of reflectance-based surface classification is limited by the low spatial resolution of intensity images, i.e. under-sampling with low point densities, and the noisy characteristics due to several factors affecting this value (Charaniya et al., 2004; Jonas, 2002; Song et al., 2002; Vosselman, 2002; Watt and Wilson, 2005).

Attempts at normalizing intensity data are presented in Donoghue et al. (2006) and Luzum et al. (2004). They compensate for variations in path lengths (ranges), i.e. the signal strength diminishes with larger ranges. Luzum

et al. (2004) apply a signal loss of one over range squared (which is justified for extended targets as detailed in Section 2.2). The values are normalized to a user-defined standard range (Eq. (1)).

$$I(R_s) = I\frac{R^2}{R_s^2} \tag{1}$$

with $I(R_s)$ as normalized intensity value to standard range R_s, I as measured intensity value and R as range between sensor position and reflection surface of a laser shot. The corrected intensities are equivalent to the intensity values that would have been recorded if the range were the same, the defined standard range, for all points. Donoghue et al. (2006) observe only small surface elevation and therefore range changes (around 80 m) in the study area. A linear regression correction approach for intensity and range is chosen to remove the assumed linear trend for intensity versus range in the given ALS data set.[2] Coren and Sterzai (2006) suggest a method, referred to as radiometric calibration, which is done in three steps a) laser spreading loss b) incidence angle and c) air attenuation correction. An asphalted road is used as homogeneous reflecting area. After removing the geometrical influence factors on the laser amplitudes, which is not explained in detail, the atmospheric attenuation coefficient is determined by best fit of an exponential decay function including the laser-target double distance and a coefficient for the total atmospheric extinction per unit length. The used data set includes a maximum double distance difference of around 150 m, which results in a weak atmospheric effect and therefore in an uncertain parameter estimation. Coren and Sterzai (2006) generate a pseudo-reflectance map out of the corrected intensity values, and directly and solely use this information for classifying the surface into 4 groups (bare ground, grass, sparse and dense vegetation).

2.2. Physical principles of ALS intensity

The basic measuring principle of Laser Scanning (LS) refers to LaDAR (Laser Detection And Ranging), more generally known as LiDAR (Light Detection And Ranging). Laser Scanning, whether airborne or terrestrial, operates on the same physical principles as microwave radar but at shorter wavelengths (Jelalian, 1992). The radar range equation (Eq. (2)), described in Jelalian (1992) comprises the three main factors a) sensor, b) target and c) atmospheric parameters, which diminish the transmitted signal power P_t.

$$P_r = \frac{P_t D_r^2}{4\pi R^4 \beta_t^2}\eta_{sys}\eta_{atm}\sigma \tag{2}$$

where the received signal power P_r is a function of the transmitted signal power P_t, the receiver aperture diameter D_r, the range from sensor to target R, the laser beam width β_t, a system η_{sys} and atmospheric transmission factor η_{atm} and the target cross-section σ. In Eq. (2) it is assumed that i) the receiver field of view matches the beam divergence and that ii) emitter and detector have the same distance to the target.

The effective target cross-section (backscattering cross-section) σ contains all target characteristics and is defined as:

$$\sigma = \frac{4\pi}{\Omega}\rho A_s \tag{3}$$

where σ is a function of the scattering solid angle of the target Ω, the target reflectance ρ and the target area A_s. The direction of the reflection is determined by the angle between the laser beam and the target area; the angle of incidence α. It is defined as the angle enclosed by the surface normal and the laser shot direction. The reflectance is the portion of reflected to incident radiation from the target area in the laser wavelength, a value averaged over the total target area. The type of reflection (e.g. specular or diffuse) influences both the direction and the strength of the backscattering cross-section. The target size is the effective area illuminated by the laser beam, i.e. the size of the orthogonal-to-ray projected area of the scatterer (Wagner et al., 2004).

Under the following assumptions Eq. (3) can be simplified (Jelalian, 1992). Firstly, the entire footprint is reflected on one surface (extended target) and the target area A_s is circular, hence defined by the laser beam width β_t and the range R. Secondly, the target has a solid angle of π steradians ($\Omega = 2\pi$ for scattering into half sphere). Thirdly, the surface has Lambertian scattering characteristics. If incident angles are greater than zero ($\alpha > 0°$), σ has a proportionality of cos α (Jutzi and Stilla, 2006; Rees, 2001).

$$A_s = \frac{\pi R^2 \beta_t^2}{4} \tag{4}$$

$$\sigma = \pi\rho R^2 \beta_t^2 \cos\alpha. \tag{5}$$

Substituting this into the radar range equation (Eq. (2)) leads to an inverse range square dependency of the

[2] This model is an oversimplification from the physical point of view, but proofed to be sufficient for the data of that study.

received signal power (Eq. (6)), independent of the laser beam width.

$$P_r = \frac{P_t D_r^2 \rho}{4R^2} \eta_{sys} \eta_{atm} \cos\alpha. \quad (6)$$

The areas of non-extended diffuse targets show different range dependencies, as for example point targets (e.g. a leaf) with an area smaller than the footprint are range independent, and linear targets areas (e.g. wire) are linear range dependent (Jelalian, 1992). As a consequence the received power reflected from non-extended targets underlies an inverse range-dependent function with higher power ($1/R^4$,$1/R^3$).

Most ALS systems do not record the emitted power or even the emitted waveform. Hence, *stability* of the emitted laser power is the prerequisite for modeling the external factors influencing the received power. The system transmission factor η_{sys}, the *optical transmission efficiency* of all optical components in the ALS system, is assumed to be constant for a certain ALS system but may vary with different systems (and over time). The aperture diameter D is also set to be a constant factor within an ALS campaign using the same system.

The system-independent atmospheric effect expressed by η_{atm} stands for the average atmospheric conditions at the time of flight. Even if we assume the atmospheric conditions, i.e. the loss of energy primarily due to scattering and absorption of the laser photons in the atmosphere between scanner and target, to be constant for an LS campaign the range strongly influences the total amount of extinction. For a wavelength of 1.06 μm the effect of scattering considerably exceeds the contribution of absorption (Kim et al., 2001). For horizontal propagation, the attenuation a can range from 0.2 dB/km for extremely clear conditions to 3.9 dB/km for haze conditions (Jelalian, 1992). Regarding vertical paths, the atmospheric transmittance typically increases with higher altitudes, which results in lower average attenuation coefficients in comparison to horizontal paths. For flying heights of 1000 m, 2000 m and 3000 m above ground and above sea level, the average vertical attenuations are 0.22, 0.17 and 0.14 dB/km, respectively. These values hold for mid-latitude summer and rural aerosol conditions with a visibility of 25 km. For the flying height of 1000 m η_{atm} becomes 0.91 according to Eq. (7).

$$\eta_{atm} = 10^{-2Ra/10000} \quad (7)$$

with a as atmospheric attenuation coefficient in dB/km and R in meters[3].

[3] The factor 10000 originates from a given in deciBel per kilometer, whereas R is in meters as before.

The noise in the intensity measurement is around 10%, which is derived from practical experience, looking at the distribution of intensities in homogeneous regions (also reported by Ahokas et al., 2006). Under very clear atmospheric conditions and small ranges of η_{atm} could therefore be neglected. On the other hand, intensities have to be corrected, particularly when large range differences appear. Therefore, the model has to consider the range dependency of η_{atm} as well. Due to the lack of detailed meteorological data of the atmospheric layers (e.g. temperature, water vapor or aerosol concentration) and the high spatial variability of these parameters, an approximated value for a has to be chosen, which should represent the average atmospheric conditions at time of flight. This leads to the equation in the following form:

$$P_r(R) \propto \frac{\rho}{R^2} 10^{-2Ra/10000} \cos\alpha \cdot C \quad (8)$$

with factor C representing the sensor parameters (e.g. P_t,D, system losses), which are assumed to be constant within a flight campaign using the same ALS system settings.

Except for full-waveform digitizing systems a further specification of the processing steps of the received power P_r is not delivered. The left side of Eq. (8) is converted into a voltage, amplified in the ALS system and finally transformed into a digital number (DN), i.e. scaled integer value, through an unknown proprietary function. Assuming *linearity in this transformation* and the *intensity always to be the peak amplitude of the received signal*, it is further possible to compare intensity measurements. With a Gaussian pulse waveform the amplitude at a certain percentage of the pulse width delivers comparable values. The peak of a Gaussian can e.g. be found at 50% of the width. Extended single targets with almost Lambertian reflectance characteristics and unchanged reflectance have to be identified, which allows for estimating differences in the constant C between time shifted ALS campaigns. Having target areas with a defined reflectance ρ, e.g. measured by a spectrometer on the ground would even allow a direct determination of parameter C. The normalization of the intensity to an average range and the estimation of C offer a reasonable approximation of surface reflectance under the conditions explained above.

3. Data sets

The study area, about 7 km^2 of the airport of Münster/Osnabrück, is located in Northwestern Germany. The ALS campaign was carried out in the end of August 2005

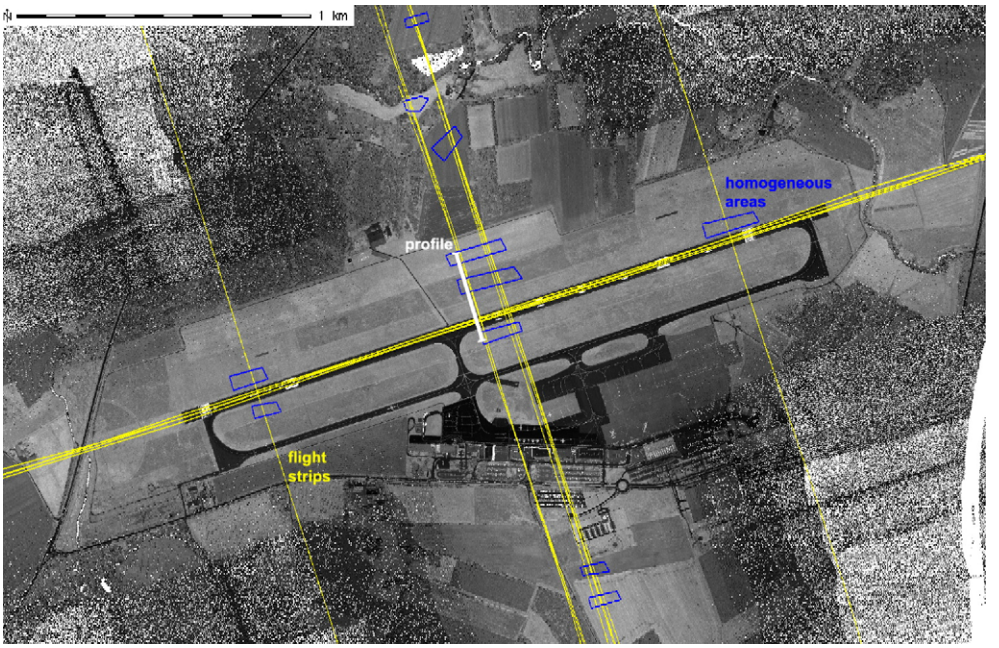

Fig. 1. Overview of study area airport Münster/Osnabrück: i) raster with maximum value of recorded intensity per cell (1 m cell size, empty cells left blank) as background image — lower point density (fewer overlapping strips) in image corners can be clearly seen; ii) flight strips, iii) selected homogeneous areas and iv) selected profile line.

by TopScan GmbH (www.topscan.de) with Optech's ALTM 3100 (www.optech.on.ca), a pulsed small-footprint system with multiple echo recording. An overview of the 18 flight lines is given in Fig. 1 and a detailed description is listed in Table 1. The ALS system employed works with a laser wavelength of 1064 nm and the intensity is digitized by 12-bit. The beam divergence was constantly set to 0.3 mrad, the maximum scan angle to ±25° and the scan frequency varies between 40 and 70 Hz. The ALTM 3100 system provides pulse repetition rates of 33, 50, 70 and 100 kHz, which are specified with different maximum flying altitudes above ground level, for example 2500 m for 50 kHz and 1100 m for 100 kHz. The ALS data is stored and processed in a database with

Table 1
Description of flight strips at Münster/Osnabrück airport used for correction experiments

Strip	Shots	Length [m]	Scan frequency [Hz]	Pulse repetition frequency [Hz]	Average intensity [DN]	Average range [m]
1	308,391	630.94	40	50,000	8.93	2542.93
2	4,031,970	5614.16	40	50,000	8.61	2557.43
3	320,162	586.93	40	50,000	7.28	2551.24
4	2,528,142	3590.61	40	50,000	8.60	2554.89
5	3,359,139	4643.69	40	50,000	8.91	2536.01
6	3,599,554	3616.55	40	70,000	17.64	1737.76
7	122,968	242.87	40	70,000	15.99	1737.68
8	181,351	294.01	40	70,000	16.83	1735.10
9	485,826	577.35	40	70,000	17.34	1739.82
10	3,005,008	2952.80	40	70,000	17.22	1733.79
11	4,581,332	4539.55	40	70,000	16.61	1735.78
12	10,048,091	7258.68	40	100,000	35.83	1027.87
13	9,356,560	7219.90	40	100,000	36.00	1022.33
14	4,540,815	3212.75	40	100,000	33.60	1018.79
15	5,220,352	3721.22	40	100,000	32.86	1027.35
16	6,335,042	4407.87	45	100,000	33.46	1006.26
17	4,811,324	3832.15	50	100,000	34.37	1012.31
18	6,177,849	4352.60	70	100,000	34.36	991.08

spatial indexing, which provides fast access to spatially distributed data (Rigaux et al., 2001). This spatial database also allows for full access to all relevant information for each ground measurement, including for example intensity, corresponding interpolated plane position and pulse repetition rate (cf. Höfle et al., 2006).

4. Methods

Two different methods for intensity correction were developed, which have different requirements for their input data sets. For both approaches the laser points (x,y,z,I) together with their corresponding plane position (x,y,z) are required for reconstruction of the laser shot vector (direction and length), which is used for calculating range and angle of incidence. The first method – data-driven correction – is suitable for flight campaigns where multiple flying altitudes are given for a part of the scanned area, not necessarily for the whole area of interest. These over-represented areas are used to estimate the parameters for the empirical correction model, which is further applied to the whole data set. Alternatively, correction parameters derived for a standard campaign may be applied to similar missions. The second method – model-driven correction – which is based on the physical model of ALS (see Eq. (8)) has less demands on the ALS data set itself but requires information about the atmospheric conditions during data acquisition.

4.1. Mathematical model and parameter estimation for data-driven correction

For the data-driven correction it is assumed that the recorded intensity is proportional to the ground reflectance and related to the flying height via a monotonic function, e.g. inversely quadratic (cf. Table 2). With this assumption, all physical effects, e.g. extinction in the atmosphere, will have an influence on the estimated parameters. This means that all effects are (partly) compensated for, too. The value of such a model is that once the parameters are obtained, the parameters can be used for further missions (with the same system settings, comparable atmospheric conditions, etc.). Additionally, error analysis can show the capabilities and limitations of the method and give hints on the validity of the assumption. Also, the method allows for the compensation of unknown or unmeasured physical effects.

Table 2
Tested empirical models (cf. Eqs. (9), (10) and (11))

Model no.	$f(r)$
1	$\frac{1}{ar^2+br+(1-1000^2a-1000b)}$
2	$ar^2+br+(1-1000^2a-1000b)$
3	$ar^3+br^2+cr+(1-1000^3a-1000^2\,b-1000c)$
4	$ar+(1-1000a)$
5	$\frac{1}{ar+(1-1000a)}$

For the estimation of the function parameters, only measurements to extended targets may be used. This means that laser shots where more than one echo was returned may not be included in the test, because it is not known which proportion of area was struck by the emitted energy. The area covered and its reflectance are two parameters that are not distinguishable in the received echo. Furthermore, it has to be assumed that the target has uniform reflectance. Therefore points measured on the border of two different materials, as well as shots with more than one echo, must not be used. The angle of incidence of the laser beam onto the reflecting surface has an influence on the backscattered energy and should therefore be constant throughout the experiment.

The general mathematical model is:

$$i(r) = i^{1000} f(r), \quad f(r) < f(r+\Delta r) \quad \forall \Delta r > 0, \qquad f(1000) = 1. \tag{9}$$

The above equation depicts the relation between observed intensity i and range r and the intensity that would be observed with a range of 1000 m i^{1000}. The requirement that the value of the function f for a range of 1000 m is one is introduced to overcome an overparametrization. Possible models for the function f are

$$f(r) = \frac{1}{ar^2+br+(1-1000^2a-1000b)} \tag{10}$$

$$f(r) = (1-1000c_1-1000^2c_2-\ldots)+c_1r+c_2r^2+\ldots. \tag{11}$$

Eq. (10) shows the inversely quadratic relation between observed intensity and flying height, whereas Eq. (11) can be seen as estimating the coefficients of the Taylor expansion of the physical function relating intensity to flying height.

In order to estimate the function parameters, points are selected in cells with homogeneous intensity within one flying strip to guarantee the requirements. For such a cell measurements from different heights (more precisely: ranges) have to be available. If the functional relationship is quadratic, at least three notably different ranges are required. Those cells, e.g. laid out in a regular

quadratic grid, which fulfill the homogeneity criterion (low standard deviation of intensities) and the different ranges requirement will be called fields in the following. The fields are indexed by the letter k.

For each field a number of observations of intensity obtained at a specific range are given:

$$\text{Field } k: \quad (i_{k,l}, r_{k,l}), \quad l = 1, \ldots b_k, k = 1, \ldots f.$$

Where f is the number of fields, b_k the number of observations in field k, and $i_{k,l}$ an observed intensity in that field. The observation equations now read:

$$\widehat{i_{k,l}} = \frac{\underline{i_k^{1000}}}{\underline{a}(r_{k,l}^2 - 1000000) + \underline{b}(r_{k,l} - 1000) + 1} \tag{12}$$

$$\widehat{i_{k,l}} = \underline{i_k^{1000}}(1 + (r_{k,l} - 1000)\underline{c_1} + (r_{k,l}^2 - 1000^2)\underline{c_2} + \ldots) \tag{13}$$

In Eqs. (12) and (13) the unknowns are underlined, the stochastic observation is displayed with a hat and the range is a known, not stochastic parameter. These are the observation equations used for estimating the unknown parameters of the functions Eqs. (10) and (11), respectively. The parameter $\underline{i^{1000}}$ is estimated per field, whereas the function parameters are global. It is also noted that with flying heights of around 1000 m the factors next to the unknowns are kept small. As the equations are not linear they have to be linearized and approximate values have to be determined for least-squares adjustment (LSA). Approximations for i_k^{1000} can be obtained by investigating the measurements in each field independently, again applying a model as Eq. (1) with $R_s = 1000$ or Eq. (12) with a and b determined for each field separately.

The number of unknowns is $2+f$, and the number of observations is the total number of all points in all fields $\Sigma_{k=1}^{f} b_k$.

4.2. Theoretical intensity correction — model-driven correction

For correcting the recorded intensity values on theoretical grounds, a number of assumptions are also made; namely, that 1) the reflectors are assumed to be extended Lambertian reflectors, 2) the surface slope can be estimated from a neighborhood of points, 3) the atmospheric conditions are known (and constant), 4) the transmitted laser power P_t is assumed to be constant (or changes in time or due to different scanner settings are known), and 5) the receiver maps incoming power linear to the recorded intensity values.

The first two assumptions are fulfilled over open terrain and can be enforced to a large extent by eliminating shots with multiple echoes. In forested areas multiple reflections are the norm, not the exception, and obtaining measures close to physical properties of the reflecting surfaces becomes impossible. If all assumptions are fulfilled, the result is a value directly proportional to ρ as defined in Section 2.2.

$$\rho_{\text{diffuse}}(R_s, \alpha) \propto I \frac{R^2}{R_s^2} 10^{2Ra/10000} \frac{1}{\cos\alpha} \tag{14}$$

with $\rho_{\text{diffuse}}(R_s,\alpha)$ as value proportional to ρ normalized on range R_s, I as recorded intensity, R as recorded range and α as angle of incidence defined as angle between surface normal and incoming laser shot ray.

With ALS data the geometry of the reflector has to be approximated. In general, the footprints of the laser shots do not overlap and therefore only one geometrical measurement (x,y,z) within the reflecting area is given. By calculating an orthogonal regression plane for a certain point neighborhood (e.g. fixed distance, k-nearest neighbors) an estimation for the real surface geometry can be used to calculate the angle of incidence of the laser ray.

In Eq. (14) the atmospheric attenuation is summarized by the coefficient a. The coefficient a has to be seen as an average value for the atmosphere between airplane and ground. One may have complex and variable atmospheric conditions during a flight campaign as well as different atmospheric layers the laser ray travels through. For simplicity and computational reasons the determination of a for each single measurement is not included in the intensity correction model. A more sophisticated meteorological model could be used to derive an average atmospheric attenuation coefficient for each laser shot, for example if information about different atmospheric layers is given. The coefficient a could be a function of R but also of the absolute elevation z, for example as the concentration of scattering particles decreases with altitude.

5. Experiments

5.1. Evaluation method of intensity correction

The primary objective of the intensity correction – to reduce variations and systematic errors due to influences of scan geometry and atmosphere – is evaluated a) on basis of a raster where the reflectance is assumed to be homogeneous for each field and b) for the flight strips where the effect of correction can be seen as *strip adjustment* for intensities. The standard deviation of the

Fig. 2. *r*-square of the local LSA for an empirical model. Low *r*-square values in the image corners are mainly due to the small number of strips covering these areas, hence resulting in a small number of points and few distinguishable ranges per cell (3 m cell size).

intensities within one field shows the degree of variation. The different data scaling when normalizing on a standard range leads to significant spreading or narrowing of the standard deviations. Therefore, the coefficient of variation c_v (S.D./mean) of the intensities before and after correction is chosen as measure of quality. Furthermore, the quality of the empirical model used in the data-driven approach is described by the root-mean-square error of the LSA. All in all, the visual inspection of the corrected intensity images clearly show the reduction of disturbance.

5.2. Data-driven correction

The data-driven correction consists of three major steps a) select fields that fulfill the criteria described in Section 4.1, b) perform the global LSA with the data collected from the accepted fields and c) apply the correction formula to all measurements. First, the whole test area has to be restricted to areas where homogeneous reflectance is expected. This can be done either manually (e.g. digitize areas, cf. Fig. 1) or automatically, for example excluding areas with multiple echoes (and therefore not extended targets, e.g. vegetation), extremely high (e.g. to avoid specular reflectors) or extremely low intensities (e.g. to avoid partial reflectors). The selected areas must include the whole spectrum of ranges and intensities to reach representative results. The size of the fields mainly depends on the given point density and on the land-cover characteristics. The fields should not be too large to cover more than one surface class but should be large enough to contain a respective sample size, i.e. number of points and distinguishable flying altitudes. For all fields that are within the expected homogeneous areas the intensity homogeneity (relative standard deviation, respectively coefficient of variation) and the number of points (>10 pts./strip) are checked per strip. Additionally, only fields with more than three different flying altitudes are accepted. For each field the empirical model (cf. Table 2) is preliminary fitted (local LSA) and analyzed by evaluating the fraction of variance in the data that is explained by the model, termed *r-square*.[4] Fields with *r*-square <0.9 are rejected. Generally, low *r*-square values mainly occur where different surface reflectances are within a field or the ranges of the laser points are poorly distributed (Fig. 2). A maximum number of accepted fields is reached for a field size of 3 m (cf. Table 3). For the parameter estimation only intensities of single echo points[5] that do not exceed an angle

[4] In statistics *r*-square is defined as *r*-square = 1 − (residual sum of squares / total sum of squares) (cf. Stein et al., 2002).

[5] Selection of shots with single echoes does not guarantee selecting extended targets only, as there is a potential of having small or dark reflectors that may generate an echo below detection threshold. In any case distinct non-extended targets are excluded.

Table 3
Comparison and evaluation of different empirical models (cf. Table 2) and field sizes for one flight campaign at Osnabrück airport, area of interest for evaluation are limited to previously selected homogeneous areas (Fig. 1)

Field size	Model	Estimation process			Evaluation process	
		Fields accept.	Points accept.	r-square	$\bar{c}_v$/field [%]	$\bar{c}_v$/strip [%]
5 m	I_{obs} [a]	2254	647,277		30.98	50.22
	1	2254	647,277	0.97	10.69	7.79
	2	2050	569,801	0.94	9.02	5.11
	3	2053	571,004	0.94	9.76	7.26
	4	1251	295,750	0.92	21.08	29.19
	5	1255	283,177	0.92	12.12	10.99
	$R^2/1000^2$				21.50	20.69
3 m	I_{obs} [a]	6266	646,549		30.91	50.17
	1	6263	646,276	0.97	10.56	8.50
	2	5738	576,503	0.94	8.87	6.03
	3	5746	577,579	0.94	9.97	9.08
	4	3803	340,545	0.92	21.33	30.01
	5	3909	341,531	0.92	12.06	11.53
	$R^2/1000^2$				21.40	21.02
1 m	I_{obs} [a]	56,341	645,932		28.51	31.73
	1	2046	42,853	0.98	9.40	9.10
	2	1935	40,563	0.95	7.75	6.86
	3	1964	41,159	0.95	11.56	12.23
	4	1608	33,736	0.93	13.69	14.84
	5	1599	33,421	0.94	10.92	11.07
	$R^2/1000^2$				19.05	20.18

The angle of incidence is not considered both in the estimation and the evaluation processes.
[a] Observed, uncorrected intensities.

of incidence of 10° are used. This minimizes the impact of the angle of incidence on the echo ($\cos(10°) > 0.98$, therefore below noise level). The result of the parameter estimation is a correction formula to normalize all intensities to a certain *range level*, a mean *r*-square for all accepted fields and the corresponding global LSA quality parameters (e.g. root-mean-square errors).

Performing a global LSA in comparison to the overall averaged least-squares solutions from each field shows only small differences in the derived model parameters. The correction functions are quite similar (see Fig. 3) and therefore analogous results are achieved. The threshold for incidence angle in the parameter estimation process should lead to a correction function not considering the effects of terrain slope (cf. Table 3). Taking into account α, i.e. topographically correcting the intensities in the evaluation process, only small changes in the results can be seen (for model 2 (5 m): $\bar{c}_v$/field = 8.90% (vs. 9.02% without α), $\bar{c}_v$/strip = 5.20% (vs. 5.11%)) due to the relatively flat terrain at Osnabrück airport. So far the evaluation process has been done for the homogeneous fields used in the estimation step (cf. Table 3). Applying the intensity correction function to the whole scene, i.e. also to inhomogeneous fields, leads as expected to higher average variation per field but still shows a significant reduction of variation (for model 2 (3 m): $\bar{c}_v$/field = 24.07%, $\bar{c}_v$/strip = 10.79%; for model 2 (5 m): $\bar{c}_v$/field = 26.42%, $\bar{c}_v$/strip = 8.81%).

5.3. Model-driven correction

The model-driven correction consists of four major parts: a) emitted energy b) spherical loss c) topographic and d) atmospheric correction. The effect of these variables on the correction results is examined. The model-driven approach is insensitive to the intensity data itself, i.e. in comparison to the empirical approach it does not compensate for systematic errors, which are in some way related to *R*. Hence, this correction separates the effects of scan geometry and atmosphere from other effects that influence the signal intensity. The physical-based approach can be applied to all laser points but it has to be considered that only corrected intensities of laser points, which fulfill the assumptions in Section 4.2, can be related to surface reflectance.

5.3.1. Emitted energy

The emitted energy is typically related to the pulse repetition rate (PRR). The higher the PRR the lower the emitted pulse energy and therefore the observed intensity value. This applies to the scanning system used in this study. It has also been reported by Chasmer et al. (2005) and Baltsavias (1999b). Assuming a constant average power and pulse duration leads to a decreasing peak

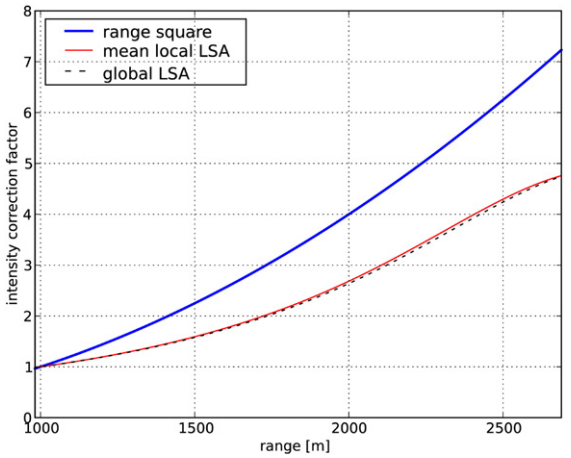

Fig. 3. Correction functions $f(r)$ i) range square (Eq. (1)), ii) averaged local and iii) global least-squares adjustment for model 2 and field size 5 m.

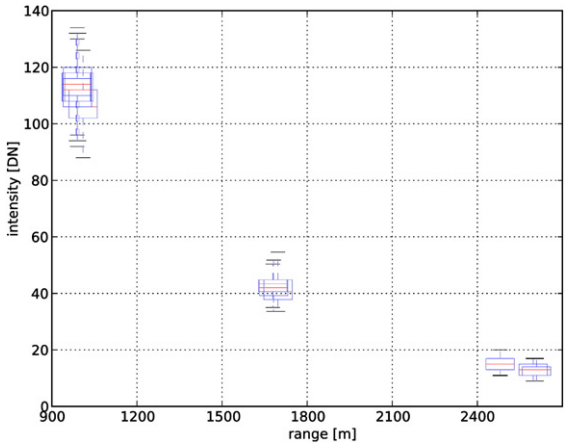

Fig. 4. Box plots of recorded intensity versus range for single flight strips for a close-cropped grass plot. The range-dependency of the intensity can be clearly seen. In this example the recorded intensities range from 9 to 136, whereas the maximum range we observed is 0 to 5100.

power indirectly proportional to the PRR settings. Therefore, Eq. (14) has to be completed by a term that corrects the influence of the PRR on the emitted power.

$$P_r(R) \propto \frac{\rho}{R^2} 10^{-2Ra/10000} \cos\alpha \frac{1}{f_{sys}} \cdot C \qquad (15)$$

with f_{sys} as factor accounting for the emitted energy. Following the equation of Baltsavias (1999b) the correction factors are $f_{sys}=1.0$ for PRR of 50 kHz, 1.4 for 70 kHz and 2.0 for 100 kHz. The values reported by Chasmer et al. (2005) for the ALTM 3100 result in correction factors of 1.0 for 50 kHz, 1.349 for 70 kHz and 1.898 for 100 kHz, which differ up to 5% from the linear approach of Baltsavias (1999b). We decided to use the values reported by Chasmer et al. (2005) as those are specific to the laser scanner model also used in our study.

5.3.2. Spherical loss

The inverse range-squared dependency of the received power of extended targets plays the major role for intensity variation in the study area because multiple flying altitudes overlap (Fig. 4), but is even evident for areas with high relief intensity and relatively constant absolute flying altitudes. Following Eq. (14) the effect of spreading loss can be removed by multiplying the original intensities by range squared divided by the normalizing range squared (e.g. $R_s=1000$ m).

5.3.3. Topographic effects

The topography is expressed by the angle of incidence of the laser ray. The incidence angles are also between ± max. scan angle for flat terrain. For ideal Lambertian scatterers the reflected intensity is proportional to cos α. The higher the portion of non-Lambertian reflectance properties (specular scattering) the smaller the amount of light coming back to the sensor if $\alpha \neq 0$. That means the assumption of having simply Lambertian scatterers can lead to a topographic overcorrection of intensities. It would be necessary to have information about the reflection characteristics of each measurement, i.e. using a high resolution land-cover classification with reflection estimates for each class, but a realistic determination still remains difficult. Following Eq. (14) the topographic effects are corrected by multiplying with 1/cos α. Fig. 5 shows the decrease of intensity towards higher incidence angles.

5.3.4. Atmospheric effects

In general, information about atmospheric conditions (e.g. Rayleigh and aerosol scattering transmittance) during a flight campaign are not available but information about the atmospheric visibility can be obtained from airport or weather data much more easily. The visibility parameter (in km) can be used as input parameter for modeling the atmospheric effect as for example with the radiative transfer model MODTRAN (Berk et al., 1998), which outputs an estimate for the integrated total atmospheric transmittance. Running MODTRAN3 with the recorded visibility of 25 km (meteorological data of airport Münster/Osnabrück), the options mid-latitude summer atmosphere and rural aerosol conditions for the three predominant flying altitudes (1070 m, 1760 m and 2560 m a.s.l. with an average target altitude of 50 m a.s.l.) results in atmospheric attenuation coefficients of 0.21 dB/km, 0.18 dB/km and 0.15 dB/km. These independent determinations can be compared to the atmospheric attenuation coefficient *a* (in dB/km) extracted from the data itself by selecting the ranges and topographically corrected intensities of a

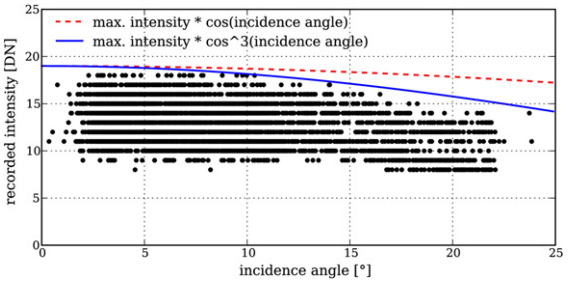

Fig. 5. Effect of incidence angle on recorded intensity for a selected cross-section of a single flight strip with constant flying altitude above ground level. Dashed line shows change of reflectance with cos α and solid line additionally includes change of range (resulting in $\cos^3 \alpha$).

Table 4
Comparison of atmospheric transmittance values for two flying altitudes: i) extracted from the data with Eq. (16) and ii) calculated with MODTRAN

Altitude [m]	η_{atm} empirical	η_{atm} MODTRAN	Rel. difference [%]
1070	0.904	0.899	−0.55
2560	0.787	0.831	5.33

homogeneous area (Eq. (16)). By dividing two equations (Eq. (15)) to the same target from two different flying heights R_1 and R_2 and corresponding angles of incidence, a can be estimated:

$$a = 5000\log_{10}\left(\frac{I_1 R_1^2 \cos\alpha_2 f_{sys1}}{I_2 R_2^2 \cos\alpha_1 f_{sys2}}\right)\frac{1}{R_2 - R_1}. \quad (16)$$

Using Eq. (16) for the flying altitudes 1070 m and 2560 m, an average value of $a = 0.20$ dB/km was determined. Using multiple fields, a standard deviation of ±0.058 dB/km was derived. Comparison of values and their agreement is shown in Table 4.

6. Results and discussion

The data-driven correction approach, exemplified by empirical model 2, shows a significant reduction of disturbance in the intensity signal (Fig. 6). After correction the variation within the homogeneous fields is reduced to $\bar{c}_v$/field <10% of the average value and the displacement between the flight strips ($\bar{c}_v$/strip) attains about 5%. The second order polynomial model accounts for all influences correlating quadratic loss (e.g. spherical) and linear loss with range. Effects related to the PRR settings, which are changed with different flying altitudes, are also compensated for. The lower PRR have higher ranges and therefore partially compensate the losses due to distance. Introducing a PRR correction

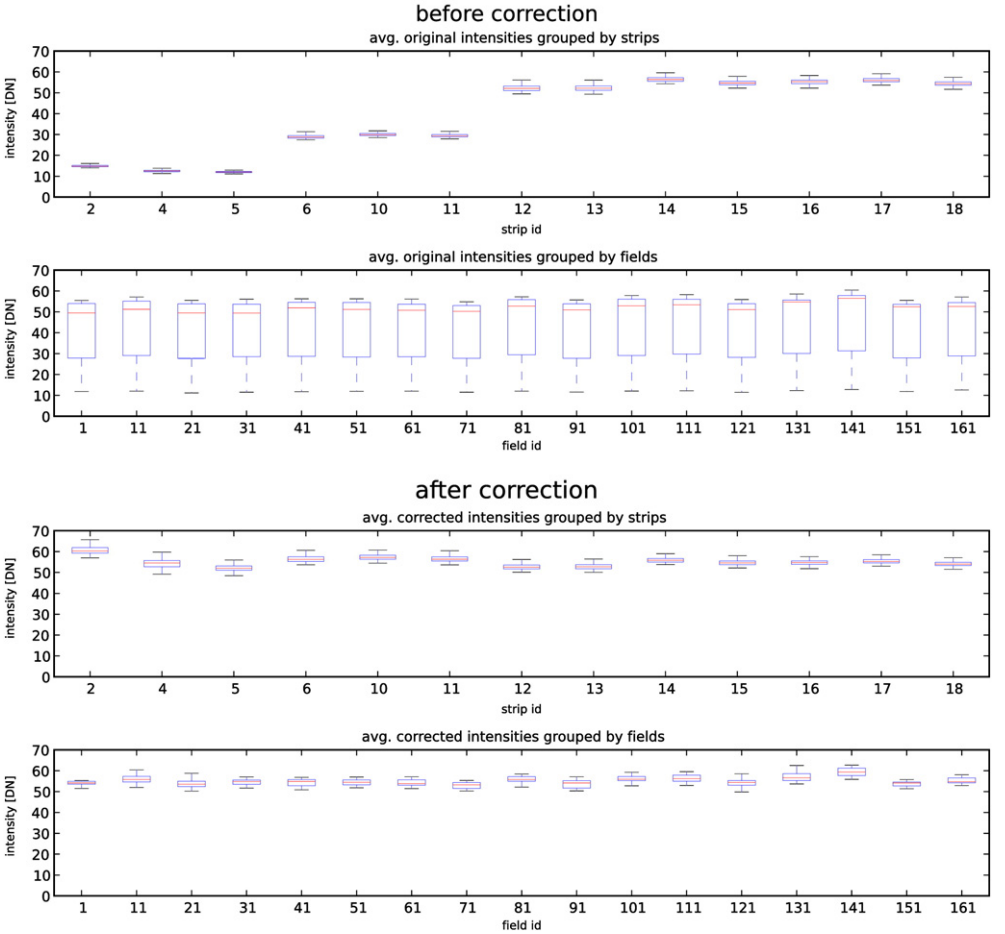

Fig. 6. Comparison of recorded and empirically corrected intensities (model 2), every 10th field (5×5 m) of a single homogeneous area.

factor before the parameter estimation delivers a correction function which has similar function values to the model-driven corrections (Fig. 7).

In the cross-sections of Fig. 8 through grass (bright) and an adjacent airstrip (dark) the successful adjustment of the single flight strips can be seen. The remaining variation originates from the inherent random noise in the intensity measurement, especially for short ranges with a small sampling area, but also from the present surface characteristics. One can easily distinguish between grass land, road and road marking. A few points from the road lying within the intensity domain of grass seem to be partially reflected from the bright marking and the dark road. In this special case calculating a mean intensity image can cause problems for surface classification, but additionally using an image with the standard deviations could provide support. The averaged intensity images (Fig. 9) clearly demonstrate the effect of intensity correction. The highest correction factors are reached for areas covered with only one high flight strip (at image corners). In Fig. 10 one can also see the boundaries of the flight strips indicated by a higher correction towards higher scan angles (cf. Fig. 1).

Performing the evaluation process with the model-driven correction procedure, considering only the spherical loss, shows a decreasing variation (1 m fields: $\overline{c}_v$/field = 19.05%, $\overline{c}_v$/strip = 20.18%) in comparison to the original intensities, but a significantly higher variability than the empirical correction. Using PRR correction factors in the correction for spherical loss and topography, as well as applying an atmospheric attenuation coefficient of 0.20 dB/km, which was estimated from the data, results in $\overline{c}_v$/field = 9.08% and $\overline{c}_v$/strip = 8.56%.

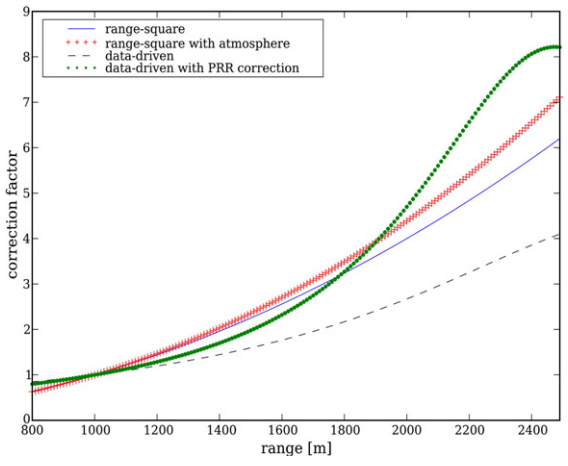

Fig. 7. Comparison of correction functions: Empirical functions are based on empirical model 2; atmospheric attenuation a set to 0.20 dB/km.

Intensity outliers directly influence the model-driven corrected intensity value. In comparison to the empirical parameter estimation process that suppresses the influence of intensity outliers, the model-driven correction does not check the values for reliability because every measurement is treated individually. Hence, using the same evaluation process as for the data-driven results further checks have to be considered (e.g. variation of intensity within each strip).

The theoretical correction can be developed further by using *radiometric control points*. This is one method of obtaining absolute ρ values. An alternative would be recording the emitted shot with the same method and obtaining ρ via the quotient of the emitted and received intensity. In order to make two campaigns, possibly with different scanners using the same wavelength, comparable, *radiometric tie points* are sufficient.

Both presented correction methods show similar results according to the reduction of intensity variation. The main differences are the data requirements. Both methods obviously need the plane position to derive the *range* and the surface normal vector to derive the *angle of incidence* for each laser shot. The data-driven correction only succeeds if multiple flying altitudes over relatively homogeneous areas are given. No further knowledge about system settings and atmospheric conditions have to be available. However, applying the correction formula is only reliable if an ALS mission is accomplished where the conditions are in the domain of the parameters used for the correction formula derivation (flying height envelope, system used, etc.). The model-driven approach primarily handles each measurement individually. Good results are achieved if P_t is constant or known, the atmospheric model reproduces the predominant atmospheric conditions at time of flight and the reflectance properties are similar to single extended Lambertian scatterers, i.e. the type of reflection and the effective reflecting area can be modeled.

The corrected intensity values are used to generate intensity images with lower systematic errors (Fig. 9). For the rasterization further constraints can be introduced to minimize the influence of intensity outliers (e.g. partial or specular reflectors), such as giving higher weight to values with lower incidence angles or ignore values outside an accepted homogeneity criterion (e.g. deviation to median value) for calculating the average cell value. Complementary to the undisturbed intensity images the information about intensity variation and outliers could be used as an additional variable for describing and classifying surface characteristics.

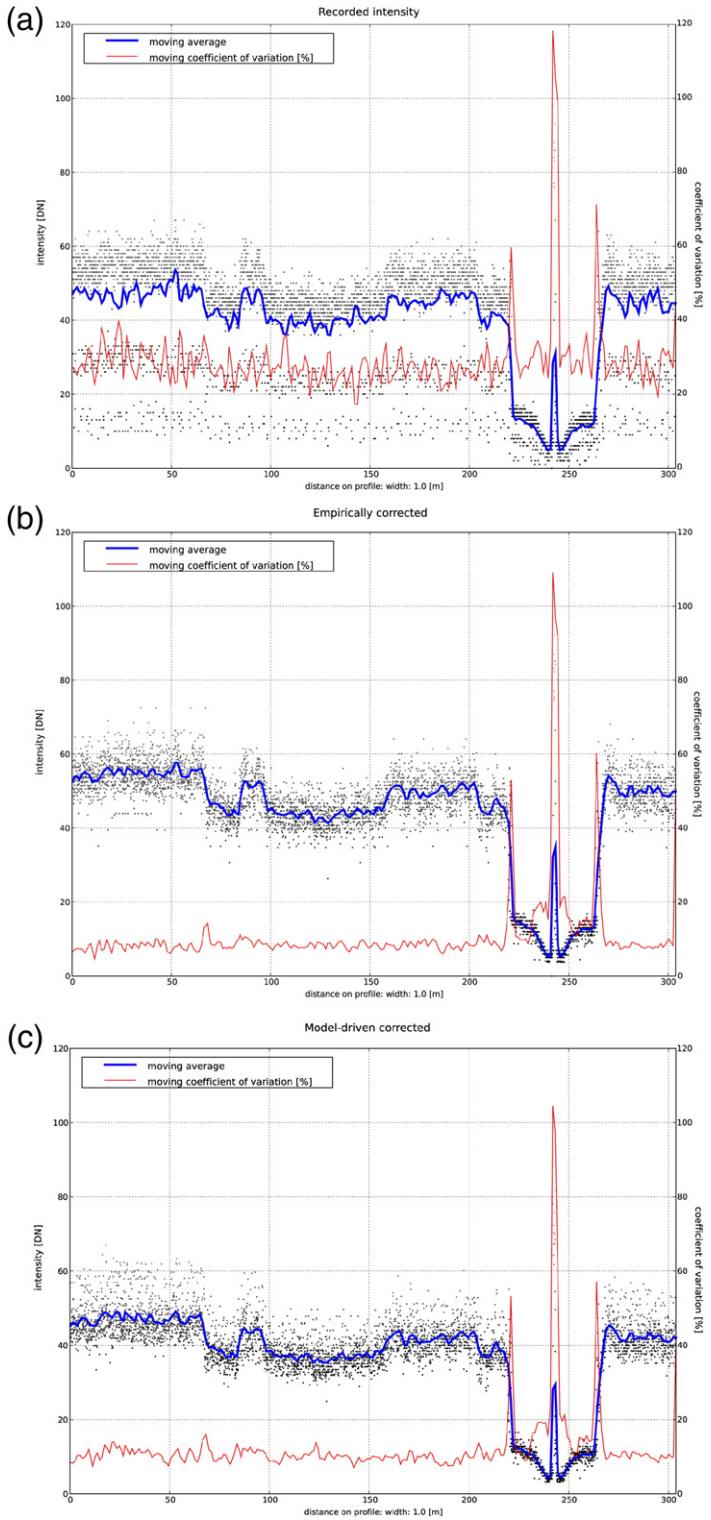

Fig. 8. Selected profile line (cf. Fig. 1) through a) recorded intensity, b) empirically corrected intensity and c) model-driven corrected intensity with moving average and coefficient of variation for each cross-section.

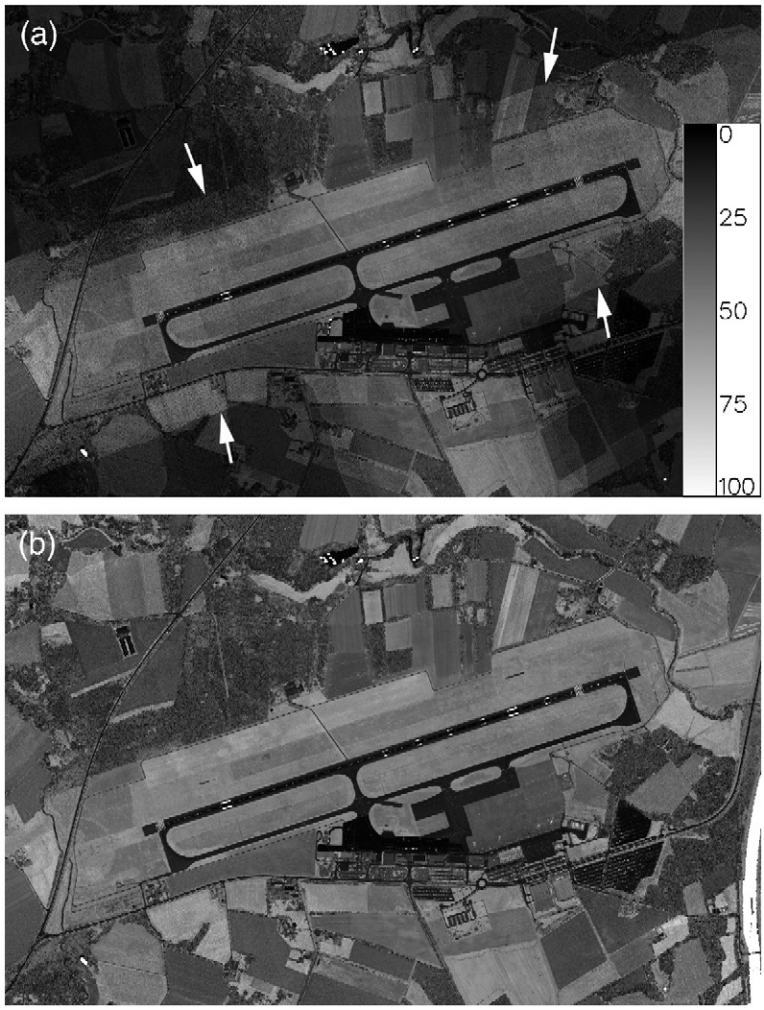

Fig. 9. Averaged intensity rasters (gray-scaled), empty cells filled with a median filter: a) original recorded intensity and b) data-driven corrected intensity.

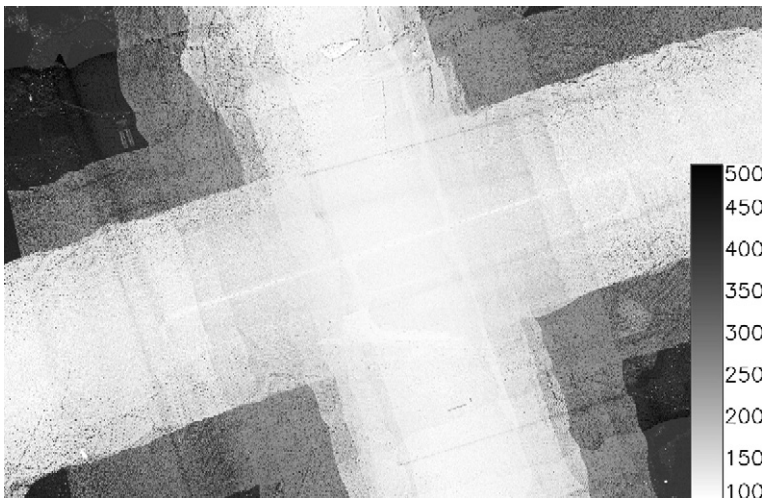

Fig. 10. Corrected intensity in percentage of original intensity.

7. Conclusions

In this paper two independent methods for correcting airborne laser scanning intensities were presented. The first approach – data-driven method – performs a least-squares adjustment for a given empirical model including intensity and range, the major variable influencing the received signal intensity. The best results were achieved with a model representing a range-square dependency. The second approach – model-driven method – is derived from the radar equation, which describes the loss of emitted pulse power. Both correction methods achieve a significant reduction of local intensity variation within cells of a regular grid (1 m, 3 m and 5 m size) spanned over the study area and an even more significant global adjustment of the single flight strips.

The evaluation of the theoretical correction showed comparable results with the empirical method. Which method to chose primarily depends on the existing ALS data set. Both methods are designed to work on large data sets. The data-driven approach solely requires multiple flying altitudes over relatively homogeneous areas. By contrast, the model-driven approach can be applied without any special requirements on the design of the flight campaign. It is therefore preferred. Eq. (15) can be used with values from atmospheric models to obtain values proportional to surface reflectance from laser scanning intensity values. Additionally, Eq. (15) can be used to estimate a (the atmospheric attenuation coefficient) or f_{sys} (a factor accounting for the emitted power) by a least squares adjustment if measurements over homogeneous areas are available from different systems or flying heights.

In high mountainous glaciated areas where optical imagery has its problems (e.g. shadows, lack of texture) intensity images have great potential to support the primary topographic information for surface classification. With the help of intensity correction the influence of relief changes are removed from the intensity value leading to an intensity map useful for glacial surface classification (Lutz et al., 2003). Having a standardized intensity correction method makes it possible to compare multi-temporal intensity data sets flown with the same scanner (e.g. monitoring of snow cover changes). If unchanged and homogeneous reflecting areas are available in the temporal shifted data sets, adjusting the intensities of different epochs is straightforward (e.g. linear regression of expected homogeneous areas to determine difference in factor C in Eq. (8)).

The paper has demonstrated that intensity values that come from ALS sensors using an unknown proprietary function to preprocess the signal can be successfully corrected. This can potentially support surface classification and monitoring of surfaces which have a good separability in the wavelength of the ALS system. Better technical information from the manufacturers should overcome the problem of changes in emitted power. However, as the power (and pulse shape) may not necessarily be constant from one shot to the next, simultaneous recording of the emitted pulse energy distribution and full-waveform digitization of the received pulse will improve the correction of airborne laser scanning intensity measurements.

With full-waveform ALS data more explicit insight into the received pulse energy is available. The peak amplitude and the pulse width can be extracted in the post-processing step with a function visible for the user. Together with the recorded emitted waveform the target reflectance ρ can be calculated with less assumptions concerning the system parameters. But the effective reflecting area (e.g. occluded areas with multiple echoes) and the scattering characteristics (e.g. Lambertian, quasi-Lambertian, specular) of the targets still remain unknown and may cause uncertainties in deriving area-wide reflectance maps from ALS.

Concerning laser range data acquired from terrestrial platforms, it has to be noted that current commercial systems do not offer the option to record more than one echo or the full-waveform. Therefore, the selection of homogeneous areas with exclusively extended targets would have to be adapted. Apart from that, and considering that the methods described in this paper work on the original point cloud, the methods can be applied to Terrestrial Laser Scanning as well.

Acknowledgments

The authors would like to thank TopScan GmbH, especially J. Lindenberger, for their cooperation in the data acquisition campaigns and providing detailed insight into ALS data processing steps.

References

Ahokas, E., Kaasalainen, S., Hyyppä, J., Suomalainen, J., 2006. Calibration of the Optech ALTM 3100 laser scanner intensity data using brightness targets. International Archives of Photogrammetry, Remote Sensing and Spatial Information Sciences 36 (Part 1). on CDROM.

Baltsavias, E.P., 1999a. A comparison between photogrammetry and laser scanning. ISPRS Journal of Photogrammetry and Remote Sensing 54 (2–3), 83–94.

Baltsavias, E.P., 1999b. Airborne laser scanning: basic relations and formulas. ISPRS Journal of Photogrammetry and Remote Sensing 54 (2–3), 199–214.

Berk, A., Bernstein, L.S., Anderson, G.P., Acharya, P.K., Robertson, D.C., Chetwynd, J.H., Adler-Golden, S.M., 1998. MODTRAN cloud and multiple scattering upgrades with application to AVIRIS. Remote Sensing of Environment 65 (3), 367–375.

Burman, H., 2000. Adjustment of laserscanner data for correction of orientation errors. International Archives of Photogrammetry, Remote Sensing and Spatial Information Sciences 33 (Part B3/1), 125–132.

Charaniya, A.P., Manduchi, R., Lodha, S.K., 2004. Supervised parametric classification of aerial lidar data. IEEE Workshop on Real Time 3D Sensor and their Use, Washington DC. June 2004. 8p. URL: http://www.soe.ucsc.edu/~amin/research/cvpr04.pdf (Accessed May 23, 2007).

Chasmer, L., Hopkinson, C., Smith, B., Treitz, P., 2005. Examining the influence of laser pulse repetition frequencies on conifer forest canopy returns. Proceedings of the Silviscan Conference, Blacksburg, Virginia, USA. URL: http://cears.fw.vt.edu/silviscan/presentations/Author24.pdf (Accessed May 23, 2007).

Clode, S.P., Rottensteiner, F., 2005. Classification of trees and powerlines from medium resolution airborne laserscanner data in urban environments. Proceedings of the APRS Workshop on Digital Image Computing (WDIC), Brisbane, Australia, pp. 191–196. URL: http://www.aprs.org.au/wdic2005/fullproceedings.pdf (Accessed May 23, 2007).

Clode, S.P., Kootsookos, P., Rottensteiner, F., 2004. The automatic extraction of roads from lidar data. International Archives of Photogrammetry, Remote Sensing and Spatial Information Sciences 35 (Part B3), 231–236.

Clode, S.P., Rottensteiner, F., Kootsookos, P., 2005. Improving city model determination by using road detection from lidar data. International Archives of Photogrammetry, Remote Sensing and Spatial Information Sciences 36 (Part 3/W24), 159–164.

Coren, F., Sterzai, P., 2006. Radiometric correction in laser scanning. International Journal of Remote Sensing 27 (15–16), 3097–3104.

Donoghue, D., Watt, P., Cox, N., Wilson, J., 2006. Remote sensing of species mixtures in conifer plantations using LiDAR height and intensity data. Oral presentation at International Workshop 3D Remote Sensing in Forestry, Vienna, February. URL: http://www.rali.boku.ac.at/fileadmin/_/H857-VFL/workshops/3drsforestry/presentations/6a.5-donoghue.pdf (Accessed May 23, 2007).

Filin, S., 2003. Recovery of systematic biases in laser altimetry data using natural surfaces. Photogrammetric Engineering and Remote Sensing 69 (11), 1235–1242.

Filin, S., Pfeifer, N., 2006. Segmentation of airborne laser scanning data using a slope adaptive neighborhood. ISPRS Journal of Photogrammetry and Remote Sensing 60 (2), 71–80.

Höfle, B., Rutzinger, M., Geist, T., Stötter, J., 2006. Using airborne laser scanning data in urban data management— set up of a flexible information system with open source components. Proceedings UDMS 2006: Urban Data Management Symposium, Aalborg, Denmark, pp. 7.11–7.23. on CDROM.

Hug, C., Wehr, A., 1997. Detecting and identifying topographic objects in laser altimeter data. International Archives of Photogrammetry, Remote Sensing and Spatial Information Sciences 32 (Part 3–4/W2), 19–26.

Hyyppä, J., Hyyppä, H., Litkey, P., Yu, X., Haggrén, H., Rönnholm, P., Pyysalo, U., Pitkänen, J., Maltamo, M., 2004. Algorithms and methods of airborne laser-scanning for forest measurements. International Archives of Photogrammetry, Remote Sensing and Spatial Information Sciences 36 (Part 8/W2), 82–88.

Jelalian, A.V., 1992. Laser Radar Systems. Artech House, Boston London.

Jonas, D., 2002. Airborne laser scanning: developments in intensity and beam divergence. Proceedings of the 11th Australasian Remote Sensing and Photogrammetry Conference, Brisbane, Australia, September.

Jutzi, B., Stilla, U., 2006. Range determination with waveform recording laser systems using a Wiener Filter. ISPRS Journal of Photogrammetry and Remote Sensing 61 (2), 95–107.

Kaartinen, H., Hyyppä, J., Gülch, E., Vosselman, G., Hyyppä, H., Matikainen, L., Hofmann, A.D., Mäder, U., Persson, Å., Söderman, U., Elmqvist, M., Ruiz, A., Dragoja, M., Flamanc, D., Maillet, G., Kersten, T., Carl, J., Hau, R., Wild, E., Frederiksen, L., Holmgaard, J., Vester, K., 2005. Accuracy of 3D city models: EuroSDR comparison. International Archives of Photogrammetry, Remote Sensing and Spatial Information Sciences 36 (Part 3/W19), 227–232.

Kager, H., 2004. Discrepancies between overlapping laser scanning strips — simultaneous fitting of aerial laser scanner strips. International Archives of Photogrammetry, Remote Sensing and Spatial Information Sciences 35 (Part B1), 555–560.

Kaasalainen, S., Ahokas, E., Hyyppä, J., Suomalainen, J., 2005. Study of surface brightness from backscattered intensity: calibration of laser data. IEEE Geoscience and Remote Sensing Letters 2 (3), 255–259.

Kim, I.I., McArthur, B., Korevaar, E., 2001. Comparison of laser beam propagation at 785 nm and 1550 nm in fog and haze for optical wireless communications. Proceedings of SPIE, The International Society for Optical Engineering 4214, 26–37. URL: http://www.systemsupportsolutions.com/WhitePapers/Comparison_Of_Beam_in_Fog.pdf (Accessed May 23, 2007).

Kraus, K., Briese, C., Attwenger, M., Pfeifer, N., 2004. Quality measures for digital terrain models. International Archives of Photogrammetry, Remote Sensing and Spatial Information Sciences 35 (Part B2), 113–118.

Lim, K., Treitz, P., Baldwin, K., Morrison, I., Green, J., 2003. Lidar remote sensing of biophysical properties of tolerant northern hardwood forests. Canadian Journal of Remote Sensing 29 (5), 658–678.

Lutz, E., Geist, T., Stötter, J., 2003. Investigations of airborne laser scanning signal intensity on glacial surfaces — Utilizing comprehensive laser geometry modeling and orthophoto surface modeling (A case study: Svartisheibreen, Norway). International Archives of Photogrammetry, Remote Sensing and Spatial Information Sciences 34 (Part 3/W13), 143–148.

Luzum, B.J., Starek, M., Slatton, K.C., 2004. Normalizing ALSM intensities. Geosensing Engineering and Mapping (GEM) Center Report No. Rep 2004-07-001, Civil and Coastal Engineering Department, University of Florida. 8 pp. URL: http://www.aspl.ece.ufl.edu/reports/GEM_Rep_2004_07_001.pdf (Accessed May 23, 2007).

Luzum, B.J., Slatton, K.C., Shrestha, R.L., 2005. Analysis of spatial and temporal stability of airborne laser swath mapping data in feature space. IEEE Transactions on Geoscience and Remote Sensing 43 (6), 1403–1420.

Maas, H.-G., 2001. On the use of pulse reflectance data for laserscanner strip adjustment. International Archives of Photogrammetry, Remote Sensing and Spatial Information Sciences 34 (Part 3/W4), 53–56.

Maas, H.-G., 2002. Methods for measuring height and planimetry discrepancies in airborne laserscanner data. Photogrammetric Engineering and Remote Sensing 68 (9), 933–940.

Matikainen, L., Hyyppä, J., Hyyppä, H., 2003. Automatic detection of buildings from laser scanner data for map updating. International Archives of Photogrammetry, Remote Sensing and Spatial Information Sciences 34 (Part 3/W13), 218–224.

Moffiet, T., Mengersen, K., Witte, C., King, R., Denham, R., 2005. Airborne laser scanning: exploratory data analysis indicates potential variables for classification of individual trees or forest stands according to species. ISPRS Journal of Photogrammetry and Remote Sensing 59 (5), 289–309.

Oude Elberink, S., Maas, H.-G., 2000. The use of anisotropic height texture measures for the segmentation of laserscanner data. International Archives of Photogrammetry, Remote Sensing and Spatial Information Sciences 33 (Part B3/2), 678–684.

Persson, Å., Söderman, U., Töpel, J., Ahlberg, S., 2005. Visualization and analysis of full-waveform airborne laser scanner data. International Archives of Photogrammetry, Remote Sensing and Spatial Information Sciences 36 (Part 3/W19), 103–108.

Persson, Å., Holmgren, J., Söderman, U., 2006. Identification of tree species of individual trees by combining very high resolution laser data with multispectral images. Proceedings of International Workshop 3D Remote Sensing in Forestry, Vienna, February, pp. 91–96.

Rees, W.G., 2001. Physical Principles of Remote Sensing, Second edition. Cambridge University Press, Cambridge.

Rigaux, P., Scholl, M., Voisard, A., 2001. Spatial Databases with Application to GIS. Morgan Kaufmann Publishers, San Francisco.

Rottensteiner, F., Trinder, J., Clode, S., Kubik, K., 2005. Using the Dempster Shafer method for the fusion of LIDAR data and multispectral images for building detection. Information Fusion 6 (4), 283–300.

Sithole, G., Vosselman, G., 2004. Experimental comparison of filter algorithms for bare-Earth extraction from airborne laser scanning point clouds. ISPRS Journal of Photogrammetry and Remote Sensing 59 (1–2), 85–101.

Song, J.-H., Han, S.-H., Yu, K., Kim, Y.-I., 2002. Assessing the possibility of land-cover classification using lidar intensity data. International Archives of Photogrammetry, Remote Sensing and Spatial Information Sciences 34 (Part 3B), 259–262.

Stein, A., van der Meer, F.D., Gorte, B.G.H., 2002. Spatial Statistics for Remote Sensing. Kluwer Academic Publishers, Dordrecht.

Thiel, K.-H., Wehr, A., 1999. Calibration procedures of the imaging laser altimeter and data processing. Proceedings of the Joint Workshop of ISPRS WGs I/1,I/3, and IV/4: Sensors and Mapping from Space, Hannover, September. on CDROM.

Vosselman, G., 2002. On the estimation of planimetric offsets in laser altimetry data. International Archives of Photogrammetry, Remote Sensing and Spatial Information Sciences 34 (Part 3A), 375–380.

Wagner, W., Ullrich, A., Melzer, T., Briese, C., Kraus, K., 2004. From single-pulse to full-waveform airborne laser scanners: potential and practical challenges. International Archives of Photogrammetry, Remote Sensing and Spatial Information Sciences 35 (Part B3), 201–206.

Wagner, W., Ullrich, A., Ducic, V., Melzer, T., Studnicka, N., 2006. Gaussian decomposition and calibration of a novel small-footprint full-waveform digitising airborne laser scanner. ISPRS Journal of Photogrammetry and Remote Sensing 60 (2), 100–112.

Watt, P., Wilson, J., 2005. Using airborne light detection and ranging (LiDAR) to identify and monitor the performance of plantation species mixture. Proceedings of ForestSat 2005, Borås, Sweden, pp. 51–55.

Wolfe, W.L., Zissis, G.J., 1993. The infrared handbook. Environmental Research Institute of Michigan, IRIA Series in Infrared and Electro Optics, Ann Arbor, MI.